Exploration of nanofluid pool boiling and deposition on a horizontal cylinder in Eulerian and Lagrangian frames

Mostafa Mahdavi, Mohsen Sharifpur* and Josua P. Meyer

*Corresponding author

*Tel: +27 12 420 2448 *Email: mohsen.sharifpur@up.ac.za

Department of Mechanical and Aeronautical Engineering, University of Pretoria,

Private Bag X20, Hatfield, 0028, Pretoria, South Africa

Abstract

In spite of many advantages of using nanoparticles in convective heat transfer, there are still some hidden aspects of nanofluids regarding simulations. Pool boiling flows are complicated regarding analytical aspects, and the presence of particles can noticeably extend this complexity. One of the most important aspects of nanofluid pool boiling is concerned with the changes in nucleation site and bubble diameter due to particles deposition and surface roughness. To include these effects, new correlations are implemented as a user-defined function for nucleation site density and bubble departure diameter. On the other hand, the particles are introduced and tracked everywhere in the domain in the Lagrangian frame by using discrete model. As an application, a tube bundle with four tubes is considered with different orientation angles concerning each other and different pitch distances. Unsteady Eulerian two-fluid model in ANSYS-Fluent is employed to simulate the liquid and vapour flows in the computational domain. In this work, pool boiling nanofluid flow is numerically solved around a two-dimensional horizontal cylinder with 20 mm diameter and compared with experimental data. The nanofluid is consist of distilled water and aluminium oxide with a particle size of 38 nm. The good agreement is found, and further discussion regarding

particles migration and deposition are presented. It is found that the percentage of deposition is dependent on heat flux and particle concentration. Also, heat transfer coefficient increases with expanding the horizontal distance between cylinders and then decreases to a fixed value.

Keywords: pool boiling, Eulerian model, discrete model, ANSYS-Fluent, nanofluids, nanoparticles

1 Introduction

Mixing of liquids via ultrafine solid particles can result in heat transfer enhancement in heat exchangers and other industrial equipment. This enhancement connected to different mechanisms which the most important one is referred to improvement in thermal conductivity of the mixture [1–3]. On the other hand, since the increase in mixture viscosity is inevitable, improvement of final thermal efficiency is connected to the optimum range of the volume fraction of the nanoparticles [4–7] which can vary from a nanofluid to another. Due to the extensive area of applications, nanofluids can be used in flows with and without phase change. Laminar and turbulent forced convection in pipes and heat exchangers are some of the common examples with no phase change flows [8,9]. Using ultrafine particles in boiling flows has attracted great attention in recent years [10,11], with the particular application in pressurized and boiling nuclear reactors. Experimental observations show both enhancement and worsening of heat transfer coefficient using nanoparticles, depending on the type and size of the nanoparticles, type of the stabilizer, base fluid and flow regime, geometry and surface roughness [12,13]. Due to the complexity and many phenomena involved in pool boiling flows, especially with the presence of solid nanoparticles, the number of numerical work is limited, and most of the previous studies cover experimental measurements and visualization.

You and Kim [14] showed that heat transfer coefficient remained nearly unchanged for alumina nanofluids on a flat plate in pool boiling at saturation temperature 60^{o}C. However, critical heat flux was found abnormally increased up to 200%. Kim et al. [15] conducted pool boiling experiment on a wire heater for three different nanofluids of low volume fractions <0.1%. They reported a noticeable rise in critical heat flux, deposition of a porous layer of nanoparticles on the wire, wettability improvement on the heater and consequently drop in contact angle. The contact angle was found to vary between 71^{o} to 80^{o} for nanofluid on a clean surface. They stated that contact angle could be highly influenced by considering the deposited layer (after boiling test), dropping to less than 40^{o}. Bang and Chang [16] observed deterioration in heat transfer coefficient of alumina nanofluid on a horizontal plate. The reduction in active nucleation sites in nucleate boiling was attributed to changes in surface roughness resulted by particles deposition. Zhu et al. [17] investigated nanofluid mixture properties and pool boiling on a heating wire. They stated that thermal conductivity and surface tension of the mixture played significant roles in heat transfer enhancement. The improvement in thermal conductivity and surface tension were measured 5% and 7%, respectively. They also reported the change in viscosity was negligible. On the other hand, they argued that the extreme increase in critical heat flux can be possibly concerned to the enhanced thermal conductivity, surface tension and the porous coating layer on the wire. Hu et al. [10] carried out nanofluids pool boiling experiment on a horizontal cylinder with ethylene glycol/water mixture as the base fluid. Particle size and volume fraction were presented as the contributing factors in rising and dropping of the heat transfer. Shoghl et al. [13] argued that any modification in heat transfer in nanofluid pool boiling is associated with the type and size of particles and also roughness of the surface caused by particles. Wang et al. [18] proposed a new correlation for the Nusselt number in pool boiling nanofluid based on the properties of the base fluid and the mixture.

On the theoretical aspect, Ham and Cho [19] studied the effects of various parameters on heat transfer, bubble departure frequency and diameter, waiting time ratio and nucleate site density. They used previous correlations from literature with considering the important impact of surface roughness induced by nanoparticles coating. Also, variation in contact angle was found as small as 10^o up to the contact angle for pure water on a clean surface as 79^o. Wang and Wu [20] employed a semi-implicit method for moving particles regarding the tracking of bubble growth in an alumina nanofluid. They introduced particle size and volume fraction at which the optimum heat transfer and bubble departure frequency were obtained. Li et al. [21] explained that bubble departure diameter, nucleate site density and other boiling parameters need to be substituted with new correlations based on the modified surface affected by nanoparticles. They also stressed on the adjustment of heat flux phenomena in the vicinity of the surface as a part of partitioning model. Shoghl et al. [22] performed both experimental and numerical study of nanofluids boiling over a horizontal cylinder. They used VOF multiphase approach in the simulations with no interactions between liquid and vapour. Only the mass exchange arising from evaporation was considered everywhere in the two-dimensional domain. Moreover, it was shown that contact angle highly depended on the type of the particles and varying from 40^o to 110^o. The same strategy was adopted by Liu et al. [23] in a two-dimensional model with cryogenic liquid.

Literature review shows that there are many phenomena involved in pool boiling with solid nanoparticles and further theoretical aspects are needed to be investigated regarding boiling characteristics, particle migration and deposition. Additionally, experimental observations have revealed that non-homogenous distribution of particles inside the medium seems unavoidable, and especially close to a wall [24]. Accordingly, using the discrete model to track the particles in the Lagrangian frame can provide higher accuracy in prediction. On the other hand, traditional correlations for nucleate site density and bubbles diameter used by

many researchers cannot be sufficient to cover all the aspects of the presence of nanoparticles in pool boiling phenomena. Therefore, this study will attempt to implement new correlations to consider other important parameters in nanofluid pool boiling, such as surface roughness and particles size.

In this study, pool boiling of nanofluids on a cylindrical geometry is simulated by the Eulerian two-phase model. Then, a mixture of water and alumina nanoparticles with 38 nm size is injected into the domain and tracked. On the other hand, nanoparticles fill the small cavities in the wall and change the roughness. It can drastically change nucleation site density and bubble departure diameter at the wall with deposited nanoparticles. To cover this, new correlations are implemented as User Defined Function (UDF) in ANSYS-Fluent.

2 Formulation of Eulerian two-phase model

In this model, each phase is treated as a continuum, and flow equations are solved in Eulerian manner. The interphase interactions occur at the interface of two phases and appear in each phase equations. The exchange of mass between phases are included in mass balance equation, and associated source terms are added to momentum and energy equations. The fundamental governing equations are as follows [25]:

$$\frac{\partial}{\partial t}\left(\alpha_k \rho_k\right) + \nabla.\left(\alpha_k \rho_k V_k\right) = \Gamma_k \tag{1}$$

$$\begin{aligned}\frac{\partial}{\partial t}\left(\alpha_k \rho_k V_k\right) + \nabla.\left(\alpha_k \rho_k V_k V_k\right) \\ = -\alpha_k \nabla P + \nabla.\left\{\alpha_k \left[\Im_k + \Im_k^t\right]\right\} + \alpha_k \rho_k g_i + M_k \\ + \left(F_{drag} + F_{lift} + F_{dispersion} + F_{lubrication} + F_{virtual}\right)_k\end{aligned} \tag{2}$$

$$\begin{aligned}\frac{\partial}{\partial t}\left(\alpha_k \rho_k h_k\right) + \nabla.\left(\alpha_k \rho_k V_k h_k\right) = \alpha_k \frac{DP}{Dt} + \nabla.\left(q_k + q_k^t\right) \\ + E_k + \alpha_k \left(\Im_k + \Im_k^t\right) \vdots V_k\end{aligned} \tag{3}$$

where Γ_k, $\Im_k$, $\Im_k^t$, M_k, q_k, q_k^t and E_k are the rate of exchanged mass between the phases, laminar shear stress, turbulent shear stress, momentum induced by mass exchanged, laminar and turbulent heat flux and exchanged heat transfer due to mass transfer and between phases, respectively. The interaction forces at the interface consist of drag, lift, turbulent dispersion, wall lubrication and virtual mass. Definition of the forces is presented following.

Drag force by Clift et al. [26] known as Grace model:

$$F_{drag} = \frac{1}{8} A_i \frac{C_D \, Re \, \mu_k}{d_v} |V_l - V_v| (V_l - V_v) \tag{4}$$

$$C_D = max\left[min\left(C_{D_{ellipse}}, C_{D_{cap}} \right), C_{D_{Sphere}} \right] \tag{5}$$

$$\begin{cases} C_{D_{Sphere}} = \begin{cases} \dfrac{24}{Re} & Re \le 0.01 \\ 24\dfrac{\left(1+0.15\,Re^{0.687}\right)}{Re} & Re > 0.01 \end{cases} \\ C_{D_{cap}} = \dfrac{8}{3}; C_{D_{ellips}} = \dfrac{4}{3}\dfrac{g d^l}{U_t^2}\dfrac{\left(\rho_k - \rho_l\right)}{\rho_l} \end{cases} \tag{6}$$

$$\begin{cases} Re = \dfrac{\rho_k |V_l - V_v| d^l}{\mu^k} \; ; U_t = \dfrac{\mu_k}{\rho_k d_v} Mo^{-0.149} \left(J - 0.857 \right) \\ Mo = \dfrac{\left(\mu^k\right)^4 g \left(\rho_l - \rho_v\right)}{\left(\rho_k\right)^2 \sigma^3} \\ J = \begin{cases} 0.94 H^{0.757} & 2 < H \le 59.3 \\ 3.42 H^{0.441} & H > 59.3 \end{cases}; \;\; H = \dfrac{4}{3} Eo \, Mo^{-0.149} \left(\dfrac{\mu_k}{0.0009} \right)^{-0.14} \\ Eo = \dfrac{g \left(\rho_l - \rho_v\right) \left(d_v\right)^2}{\sigma} \end{cases} \tag{7}$$

where Re, Mo and Eo are phase Reynolds number, Morton number and Eotvos number, respectively. A_i is the interfacial area concentration and given as:

$$A_i = \frac{6\alpha_v(1-\alpha_v)}{d_v} \tag{8}$$

Lift force by Tomiyama [27]:

$$F_{lift} = C_L \alpha_k \rho_k \left(V_l - V_v\right) \times \left(\nabla \times V_k\right) \tag{9}$$

$$\begin{cases} min\left[0.288 tanh\left(0.121 Re\right), f\left(Eo_d\right)\right] & Eo < 4 \\ f\left(Eo_d\right) = 0.00105 {Eo_d}^3 - 0.0159 {Eo_d}^2 - 0.0204 Eo_d + 0.474 & 4 < Eo < 10 \\ -0.29 & Eo > 10 \end{cases} \tag{10}$$

$$Eo_d = \frac{g\left(\rho^k - \rho^l\right)\left(d^l\right)^2}{\sigma}\left(1 + 0.163 Eo^{0.757}\right)^{2/3} \tag{11}$$

Wall lubrication force by Antal et al. [28]:

$$F_{lubrication} = C_w \rho_k \alpha_v \left|V_l - V_v\right|^2 n_w \tag{12}$$

$$C_w = max\left(0, \frac{C_{w1}}{d^l} + \frac{C_{w2}}{y_w}\right); \; C_{w1} = -0.01; \; C_{w2} = 0.05 \tag{13}$$

Turbulence dispersion by Burns et al. [29]:

$$F_{dispersion} = C_D \frac{\mu_k^t}{\rho_k Sc_b}\left(\frac{\nabla \alpha_l}{\alpha_l} - \frac{\nabla \alpha_v}{\alpha_v}\right) \tag{14}$$

Virtual mass force by Drew and Lahey [30]:

$$F_{virtual} = 0.5 \alpha_k \rho_k \left(\frac{DV_l}{Dt} - \frac{DV_v}{Dt}\right) \tag{15}$$

Heat can be exchanged between phases through the interfacial area. This heat transfer is a part of E_k in energy equation (40), given by Ranz and Marshall [31]:

$$q_k = \frac{k_k Nu_v}{d_v}\left(T_v - T_l\right) \tag{16}$$

$$Nu_v = 2.0 + 0.6 \, Re^{1/2} \, Pr^{1/3} \tag{17}$$

2.1 Mass and heat transfer in boiling

It could be assumed that mass transfer happens in two different locations, near the wall and inside the domain. The one in the domain takes place in the interfacial area for both liquid and vapour as follows [32]:

$$\dot{m} = \frac{q_l + q_v}{h_{lv}} \tag{18}$$

$$q_l = \frac{k_l Nu_l}{d_l}\left(T_{sat} - T_l\right);\ q_v = \frac{\alpha_v \rho_v c_{p_v}}{\delta t}\left(T_{sat} - T_v\right) \tag{19}$$

h_{lv}, T_{sat} and δt denote the latent heat of evaporation, saturation temperature and time scale, respectively. The mass transfer near the wall is assumed to be a part of RPI model and explained as follows.

Since the applied heat flux is below critical heat flux of pool boiling, nucleate boiling is dominant in all the cases and RPI model developed by Kurual and Podowski [33] can be applied. Partitioned heat flux model is assumed with three modes of heat transfer at the wall boundary condition, quenching heat transfer, convective and evaporative heat transfer. The convective and evaporative heat flux are obviously stemmed from the wetted region by liquid and phase change, respectively. Quenching heat flux is caused by the averaged transient heat transfer associated with detached nucleate bubbles being replaced by liquid phase.

Convective heat flux by Del Valle and Kenning [34]:

$$q_c = h_C\left(T_w - T_l\right)(1 - A_b) \tag{20}$$

where h_C, T_w and A_b are heat transfer coefficient, wall temperature and the portion of the surface covered by nucleate bubbles, respectively.

Evaporative heat flux [21]:

$$q_e = \frac{\pi}{6} d_W^3 N_W \rho_v h_{lv} f_b \tag{21}$$

where d_w, N_w *and* f_b are bubble departure diameter, nucleate site density and frequency of bubble departure, respectively. One of the most used correlations for nucleate site density and bubble departure diameter were developed by Kocamustafaogullari and Ishii [35,36]:

$$N_W = \frac{1}{d_w^2}\left[2.157\times10^{-7}\,\bar{\rho}^{-3.2}\left(1+0.0048\bar{\rho}\right)^{4.13}\right]\left(\frac{2r_c}{d_w}\right)^{-4.4} \tag{22}$$

$$\bar{\rho} = \frac{\rho_l - \rho_v}{\rho_v}, \quad r_c = \frac{2\sigma T_{sat}}{\rho_v h_{lv}(T_w - T_{sat})} \tag{23}$$

$$d_w = 0.0012\bar{\rho}^{0.9}0.0208\theta\sqrt{\frac{\sigma}{g(\rho_l - \rho_v)}} \tag{24}$$

As can be seen, the important effects of surface roughness, the entire role of system pressure and nanoparticles are not reflected in the equations. Besides, the size of nanoparticles is normally smaller than 100 nm, which can drastically change the physical geometry of the surface by filling the small cavities of the roughness [19]. To include these parameters in equations, it is essential to implement new correlations for nucleation site density and bubble departure diameter. Therefore, two different correlations were implemented according to the absence and presence of nanoparticles. Benjamin and Balakrishnan [37] developed the following correlation for nucleation site density regarding different surface roughness without nanoparticles:

$$N_W = 218.8\,Pr_l^{1.63}\,\gamma^{-1}Rn^{-0.4}(T_w - T_{sat})^3 \tag{25}$$

where Pr_l, γ and Rn are liquid Prandtl number, surface-liquid interaction parameter and a dimensionless parameter for the roughness, respectively [37]:

$$\gamma = \sqrt{\frac{k_w \rho_w c_{p_w}}{k_l \rho_l c_{p_l}}} \tag{26}$$

$$Rn = 14.5 - 4.5\left(\frac{R_a P}{\sigma}\right) + 0.4\left(\frac{R_a P}{\sigma}\right)^2 \tag{27}$$

R_a and P are surface roughness and working pressure of the system. Li et al. [38] developed a semi-empirical correlation for nucleation site density in nanofluid based on Benjamin and Balakrishnan [37].

$$N_W = 512\, Pr_l^{1.63}\, \gamma^{-1} Rn^{-0.4} \theta^{*1.2} F\left(\frac{Ra}{d_p}\right)^{0.4} (T_w - T_{sat})^3 \tag{28}$$

Two new parameters θ^* and $F\left(\frac{Ra}{d_p}\right)$ were presented to include the effects of nanoparticles and deposition [37].

$$\theta^* = \frac{1 - cos(\theta_{nf})}{1 - cos(\theta_{bf})} \tag{29}$$

$$F\left(\frac{Ra}{d_p}\right) = \begin{cases} 0.275\left(Ra/d_p\right)^{-1.2} & 0 < Ra/d_p < 1 \\ 0.275 + 0.791\left(Ra/d_p\right)^{0.68} & Ra/d_p \geq 1 \end{cases} \tag{30}$$

where θ_{nf} and θ_{bf} are contact angles on the nano-coated surface and clean surface. Bubble departure diameter is implemented in CFD software by the following equation developed by Golorin et al. [39,40]:

$$\frac{d_w}{d_1} = 1 + \frac{d_2}{d_1} \tag{31}$$

$$d_1 = \frac{1.65 d^* \sigma}{g(\rho_l - \rho_v)} \tag{32}$$

$$d_2 = \left[\frac{15.6\rho_l}{g(\rho_l - \rho_v)}\right]^{1/3}\left[\frac{\beta_d k_l (T_w - T_{sat})}{\rho_v h_{lv}}\right]^{2/3} \quad (33)$$

where $d^* = 0.006\,mm$ and $\beta_d = 6.0$ for water.

Accordingly, mass change in the vicinity of the wall is calculated as [21]:

$$\dot{m} = \frac{q_e}{h_{lv} + c_{p_l}\left(T_{sat} - T_l\right)} \quad (34)$$

Quenching heat flux [21]:

$$q_q = C_{qw}\frac{2k_l}{\sqrt{\pi\lambda_l T_b}}\left(T_W - T_l\right) \quad (35)$$

$$T_b = \sqrt{\frac{3\rho_l d_W}{4g\left(\rho_l - \rho_v\right)}} \quad (36)$$

where λ_l and C_{qw} are liquid thermal diffusivity and bubble waiting time coefficient, respectively. Waiting time represents the delay time between the formation of bubbles and rising from the surface till next bubble.

3 Discrete modelling of particles

Particles are tracked in the Lagrangian frame, and a set of flow equations are iteratively solved in this model. Hence, a finite number of particles are tracked in each time step as a representative of other particles. Due to negligible effects of virtual mass and pressure gradient forces [41], these are not mentioned and solved in the particles equations. The Newton's equation of force balance in the Lagrangian frame for nanoparticles is written in details as follows [45]:

$$m_p \frac{du_p}{dt_p} = F_{drag} + m_p \frac{\vec{g}(\rho_p - \rho_c)}{\rho_p} + F_{lift} + F_{Magnus} + F_{thermo} + F_B \quad (37)$$

t_p is the travelling time of a nanoparticle from the point of injection till it reaches its final fate in the domain.

Drag force [45]:

$$F_{drag} = \frac{m_p}{\tau}\frac{C_D Re_p}{24 C_c}\left(V_l - u_p\right) \quad (38)$$

$$Re_p = \frac{\rho_l d_p \left|V_l - u_p\right|}{\mu_l} \quad (39)$$

Smooth spherical particles are assumed for nanoparticles and simply stokes flow (obviously $Re_p<<1$) for drag coefficient. The Cunningham slip correction factor, Cc, is used when the no-slip boundary condition for a continuum cannot be preserved over a particle or solid wall [45].

$$C_c = 1 + Kn\left[2.514 + 0.8e^{-0.55/Kn}\right] \quad (40)$$

$$Kn = \frac{\lambda}{d_p} \quad (41)$$

where Kn and λ are Knudsen number and mean free path of the fluid which is 0.3 nm for water. Since the Knudsen number in this study is much less than 0.1, we can substitute $C_c=1$.

Saffman Lift Force [42]:

$$F_{lift} = 20.3\mu_l d_p^2 (V_l - u_p)\sqrt{\frac{\dot{\gamma}\rho_l}{\mu_l}}\,\mathrm{sgn}(\dot{\gamma}) \quad (42)$$

where $\dot{\gamma}$ is the shear rate. This force is mainly used here in the analysis of particles fate after a collision with a wall.

Magnus force:

This lift force is induced by rotation of the particle around its axis in uniform flow. Magnus force can be negligible regarding the nanosize of the particles. However, it can be important if the flow is highly rotational [43].

$$F_{Magnus} = \frac{1}{2} A_p C_{ML} \rho_c \frac{\left|V_l - u_p\right|}{\left|\Omega\right|} \left[\left(V_l - u_p\right) \times \Omega\right] \tag{43}$$

$$\Omega = \frac{1}{2} \nabla \times V_l - \omega_p \tag{44}$$

$$C_{ML} = 0.45 + \left(\frac{Re_{\omega_p}}{Re_p} - 0.45 \right) exp\left(-0.05684 Re_{\omega_p}^{0.4} Re_p^{0.3}\right) \tag{45}$$

$$Re_{\omega_p} = \frac{\rho_l \left|\Omega\right| d_p^2}{4\mu_l} \tag{46}$$

where A_p and C_{ML} are projected particle surface area and rotational lift coefficient. Particle angular velocity is obtained by solving the angular momentum equation [43]:

$$I_p \frac{d\omega_p}{dt_p} = \frac{\rho_l}{2} \left(\frac{d_p}{2} \right)^5 C_\omega \Omega \tag{47}$$

$$I_p = \frac{\pi}{60} \rho_p d_p^5 \tag{48}$$

$$C_\omega = \frac{6.45}{\sqrt{Re_{\omega_p}}} + \frac{32.1}{Re_{\omega_p}} \tag{49}$$

Thermophoretic force [44]:

$$F_{thermo} = -D_T \frac{\nabla T}{T} \tag{50}$$

$$D_T = 0.78 \frac{\pi \mu_l^2 d_p}{\rho_l} \frac{k_l}{2k_l + k_p} \tag{51}$$

Brownian random force. The random motion of particles suspended in a fluid can have a significant contribution to induce and gradual fluid flow in pool boiling [45].

$$F_B = \zeta_i \sqrt{\frac{6\pi d_p \mu_l K_B T}{\Delta t_p}} \quad (52)$$

where ζ_i is the unit-variance random number produced by a Gaussian white noise process.

One of the most important aspects of tracking particles is concerned with analysing the final fate of the particle. When a solid particle is in contact with a wall, the considerable impact of the electrostatic attractive force between two solid materials needs to be taken into account. This force is compared with other interaction forces to reach the final balance of the particle. The van der Waals sticking force is defined for a particle and a plate as [46]:

$$F_{VDW} = \frac{Hd_p}{12d_0^2} \quad (53)$$

where H and d_0 are Hamaker constant and equilibrium distance between the particle and nanofluid. Due to nano-size of the particles, a simple scale analysis shows that gravitational force can be safely ignored. Also, for simplicity, only thermophoresis, lift and Brownian forces are assumed as the lift-off forces from the wall.

$$F_L = F_{lift} + F_{thermo} + F_B \quad (54)$$

A comparison between sticking and lift-off forces will provide the final fate of the particles. This is implemented as a user-defined function in the CFD software. It is noted that simulations revealed that the order of magnitude of sticking force is higher than lift-off force due to a small order of velocity in pool boiling.

3.1 Turbulent eddies on particles migration

The effects of fluctuating velocity on particles trajectory can be seen via using discrete random walk model developed by Bayazit [47]. The fluctuating velocity of an eddy is presented as:

$$u_i' = \xi\sqrt{\overline{u_i'^2}} \tag{55}$$

where ξ is the randomly distributed number from Gaussian pdf and $\sqrt{\overline{u_i'^2}} = \sqrt{2/3\kappa}$ is the root mean square of fluctuating velocity, and κ as the turbulent kinetic energy. This fluctuating velocity is considered in particle motion equation as $u_i = \bar{u}_i + u_i'$. The interaction between the eddy and the particle occurs during the minimum of two characteristic times, namely lifetime of the eddy and particle eddy crossing time. At the end of the period, a new location for the particle is calculated [48]. It is noted that random walk model is essential to be considered in particles calculation, specifically regarding the possibility of sedimentation.

4 Mixture properties

Thermo-physical properties of liquid can be noticeably affected by the presence of particles. Therefore, updated mixture properties are required to be implemented. The mixture correlation is borrowed from the model developed by Sharifpur et al. [49].

$$\rho_1 = \sum_{k=1}^{2} \varphi_k \rho_k \tag{56}$$

$$\rho_m = \frac{\rho_1}{(1-\varphi) + 8\varphi(d_p/2 + t_v)^3 / d_p^3} \tag{57}$$

$$t_v = -0.0002833(d_p/2)^2 + 0.0475\, d_p/2 - 0.1417 \tag{58}$$

$$c_{P_m} = \frac{\sum_{k=1}^{2} \varphi_k \rho_k c_{P_k}}{\rho_m} \tag{59}$$

φ is particles volume fraction in liquid. Thermal conductivity and viscosity of nanofluid by Corcione, [50] and Khanafer [51]:

$$k_m / k_l = 1 + 1.0112\varphi + 2.4375\varphi\left(\frac{47\times10^{-9}}{d_p}\right) - 0.0248\varphi\left(\frac{k_p}{0.613}\right) \quad (60)$$

$$\mu_m / \mu_l = \frac{1}{\left[1 - 34.87\left(d_p / 0.3\times10^{-10}\right)^{-0.3}\varphi^{1.03}\right]} \quad (61)$$

Surface tension is one of the critical parameters and also depends on the particles concentration. Wang and Wu [20] showed that the correlation developed by Meissner and Michaels [52] for liquid mixture could be appropriate for nanofluid:

$$\frac{\sigma_l - \sigma_m}{\sigma_l} = -7.773\times10^{-3}\ln\left(\frac{\varphi}{7.673\times10^{-7}} + 1\right) \quad (62)$$

5 Geometry description and numerical considerations

The geometry is a two-dimensional cylinder with 20 mm diameter in a saturated medium. The cylinder is assumed to be in a large saturated medium with the mixture of alumina particles of 38 nm and distilled water. For the comparison purposes, the experimental work conducted by Das et al. [53] is taken into account. New correlations for nucleation site density and bubble departure diameter are implemented in ANSYS-Fluent as UDFs. At the next step, a tube bundle is simulated with alumina nanofluid in pool boiling with four tubes at different orientation angles and horizontal pitch distances (P_x) shown in Figure 1. The ratio of pitch distance to tube diameter is 1.3.

Various types of meshes are generated and tested based on the validity of both boiling and discrete models. Since realizable k-ε was chosen as turbulence model, the fine mesh was created around the wall of the cylinder to reach y+ less than 1 for enhanced wall treatment. Eulerian-Eulerian accompanied by nucleate boiling approach was employed to simulate multiphase model in the computational domain, while the discrete model was used to track the suspended particles. The geometries are illustrated in Figure 1.

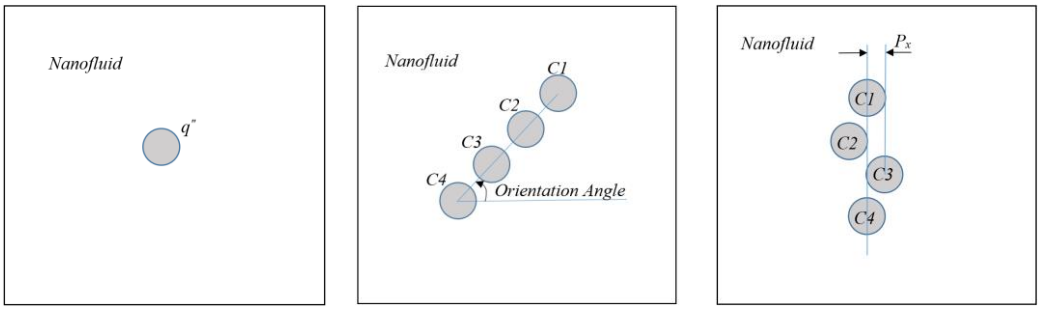

a) b) c)

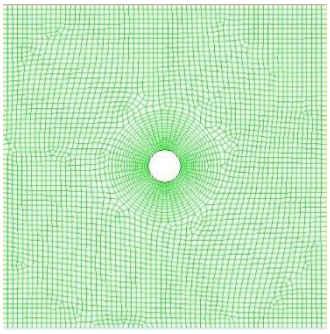

d)

Figure 1. Schematic of the geometry considered for nanofluid pool boiling

The following steps are considered in simulations:

First, the boiling flow is iteratively solved for only water and vapour with implemented nucleation site density and bubble departure diameter in ANSYS-Fluent as UDFs. This is considered 0%vol of nanofluid. Then, another correlation for nucleation site density is implemented with modified mixture properties as UDFs in the case of nanofluid. Then, alumina nanoparticles are injected into the boiling region and tracked till their final fate.

6 Results discussion

The grid study showed that the results are only sensitive to the resolution of mesh in the vicinity of the cylinder due to the formation of bubbles. However, some grid sizes were tested from 4000 cells to 80000 cells with considering superheat temperature as the criterion, and eventually, 12455 cells were chosen with fine mesh close to the cylinder. The results

remained unchanged in less than 1% error with increasing from 12455 cells. Nanoparticles are injected from the bottom of the domain and will leave the domain with water. The side boundaries are assumed symmetry, and the top boundary is pressure outlet. Also, the domain is assumed to be in the saturated liquid condition.

The validation of the simulated model is shown in Figure 2. The uncertainty of the experiment done by Das et al. [53] is around 4%, as shown in the figure with error bars of 4%. As can be seen, the simulation results are in good agreement with the experiments and in the range of uncertainty.

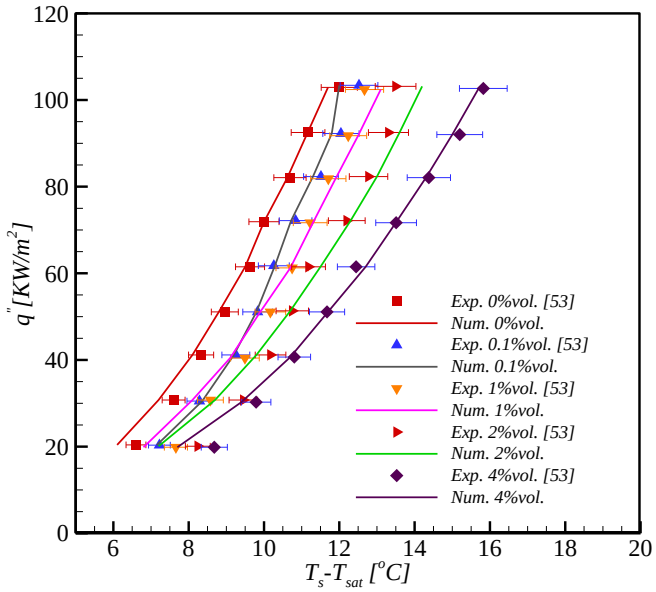

Figure 2. Superheat temperature on the wall of a horizontal cylinder in an alumina nanofluid medium

As previously mentioned, sedimentation of the particles on the wall plays a critical role in bubble formation and liquid surface tension. Due to the sophisticated phenomenon of pool boiling near to the heated wall, an estimation of particles deposition is presented in Figure 3 based on the geometry presented in Figure 1a. A comparison between the effects of nanoparticles volume fraction and wall heat flux on particles deposition reveals that there can

be conditions that the deposition reaches the maximum value and then drops. It occurs somewhere between 30 KW/m^2 to 60 KW/m^2.

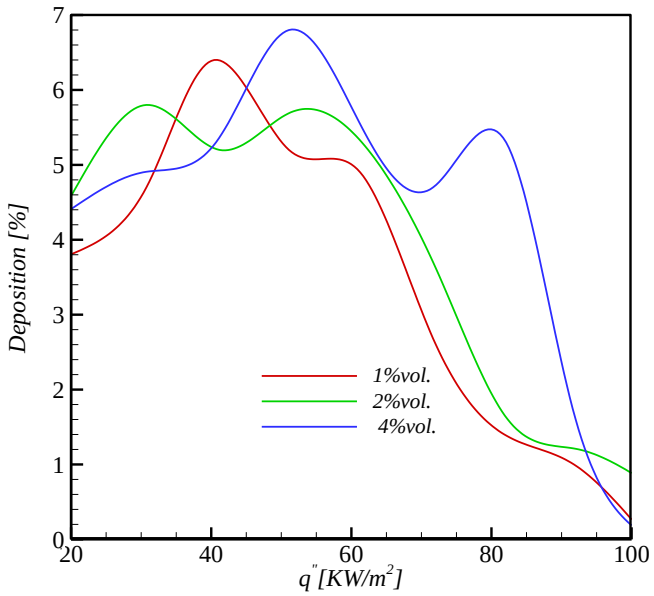

a)

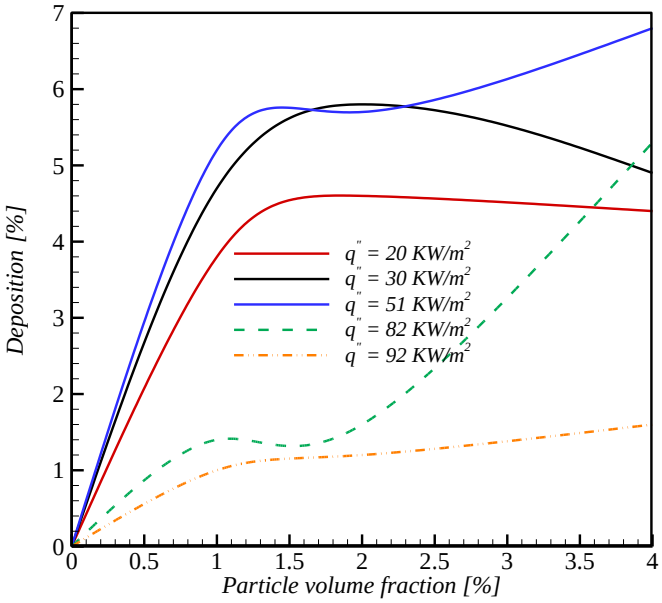

b)

Figure 3. Deposition of the alumina nanoparticles on the surface of a horizontal cylinder presented in Figure 1a.

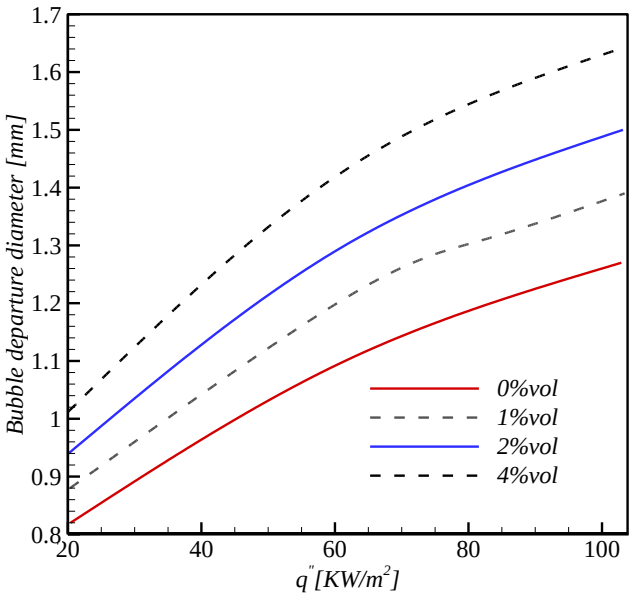

a)

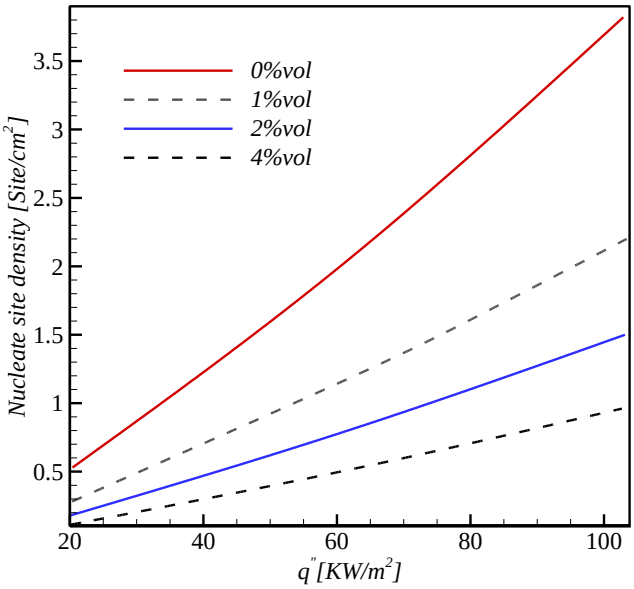

b)

Figure 4. Bubble departure diameter and nucleate site density on a cylinder in nanofluid pool boiling for geometry in Figure 1a.

Deposition sharply decreases with rising in heat flux due to increase in velocity in the vicinity of the wall and also higher steam volume fraction. It can be said that particle loading and heat

flux are the prominent factors in particles deposition. However, the up and down in results can be caused by the random nature of nanoparticles movement due to Brownian motion in the computational method. Also, the percentage varies smoothly with an increase in particle volume fraction above 1.5%vol.

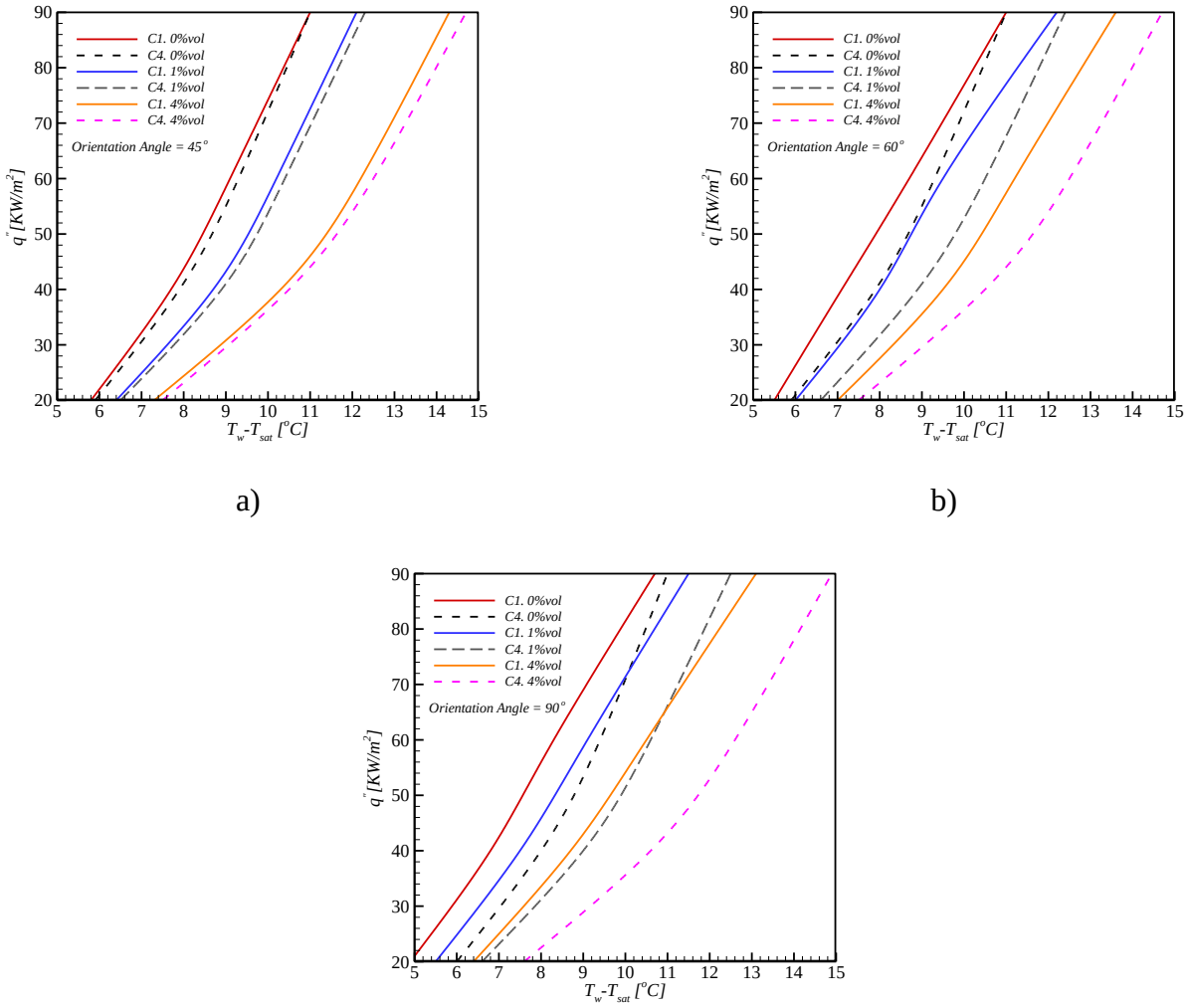

a) b)

c)

Figure 5. Water and alumina nanofluid pool boiling superheat temperature on the surface of the top tube (C1) and bottom tube (C4) at different orientation angles for geometry in Figure 1b

The evolution of bubble departure diameter and nucleate site density is presented in Figure 4 for different nanoparticles volume fraction for geometry in Figure 1a. It is observed that the

site density is noticeably affected by the presence of the particles on the surface comparing to bubble diameter.

The reason can be the pronounced effects of surface roughness and contact angle in equations (27) and (28). The change in surface tension due to nanoparticles is the most important factor in the size of bubbles diameter, included in implemented equation (31). On the other hand, nucleate site density is expected to be a function of many parameters such as surface roughness and nanoparticles diameter, included in equation (28). These parameters cause a dramatic drop in nucleate site density with increase in nanoparticles volume fraction, which can noticeably reduce the size of the roughness by filling small cavities on the surface. However, the trend is exactly opposite for site density and bubble diameter concerning increase in volume fraction.

The variation of superheat temperature and heat transfer coefficient (HTC) defined as $h = q'' / T_w - T_{sat}$ on the surface of the tubes at the top (C1 in Figure 1), and bottom (C4 in Figure 1) is shown in Figure 5 and Figure 6. Simulation results are presented for three orientation angles, 45^o, 60^o and 90^o. The effect of tube bundle is negligible for orientation angle less than 45^o, as the difference between top and bottom tubes in terms of heat transfer starts from this angle. As can be seen, superheat temperature and HTC on the top tube is always smaller and higher, respectively, than the bottom tube, even in the case of nanofluid. The magnitude of the difference increases with expanding the orientation angle due to the stronger interference of bubbles produced at bottom tubes. Increase in heat flux causes the continuous rising of HTC. The higher heat flux produces more bubbles and disturbance in the vicinity of the wall, which eventually improves the heat transfer at nucleate boiling. It means that the roles of quenching and evaporative heat flux would be prominent in heat transfer balance equation.

Bubble departure diameter and nucleate site density on the top and bottom tube are presented in Figure 7 for different particle volume fraction at 60^o orientation angle. The largest bubbles are generated at the bottom tube and higher particle volume fraction. While the size of the bubbles is smaller at the top tube due to the cooling effect of stronger flow produced by lower tubes. Also, the negative impacts of nanoparticles at higher volume fraction on heat transfer in the vicinity of the wall can be the other reason for larger bubbles. On the other hand, the amount of site density considerably decreases with increase in nanoparticles concentration. The number of sites produced at the top tube is lower because of interruption by the bubbles from other tubes. Moreover, it is observed that the slope of the site density rapidly decreases with increase in volume fraction. It can be mainly concerned with the effect of particle deposition and making the surface smoother with lower roughness, up to even 10 times smoother surface with an increase in particle concentration [13]. It is noted that the order of power in surface roughness in nucleate site density correlation is around 3, which can dramatically change the number of nucleation sites.

Due to impacts of orientation angle, the results for wall superheat temperature, and HTC on the top (C1) and bottom (C4) tubes are illustrated in Figures 8 and 9 in terms of orientation angle. Variation of orientation angle shows no effects on heat transfer on the bottom tube. However, HTC starts improving on the top tube by increasing orientation angle above 50^o. It is also observed that nanoparticles have negative impacts on heat transfer. It can be mainly attributed to the changes in boiling parameters such as bubble departure diameter and nucleate site density shown in Figure 10 due to the improved surface by nanoparticles deposition [13].

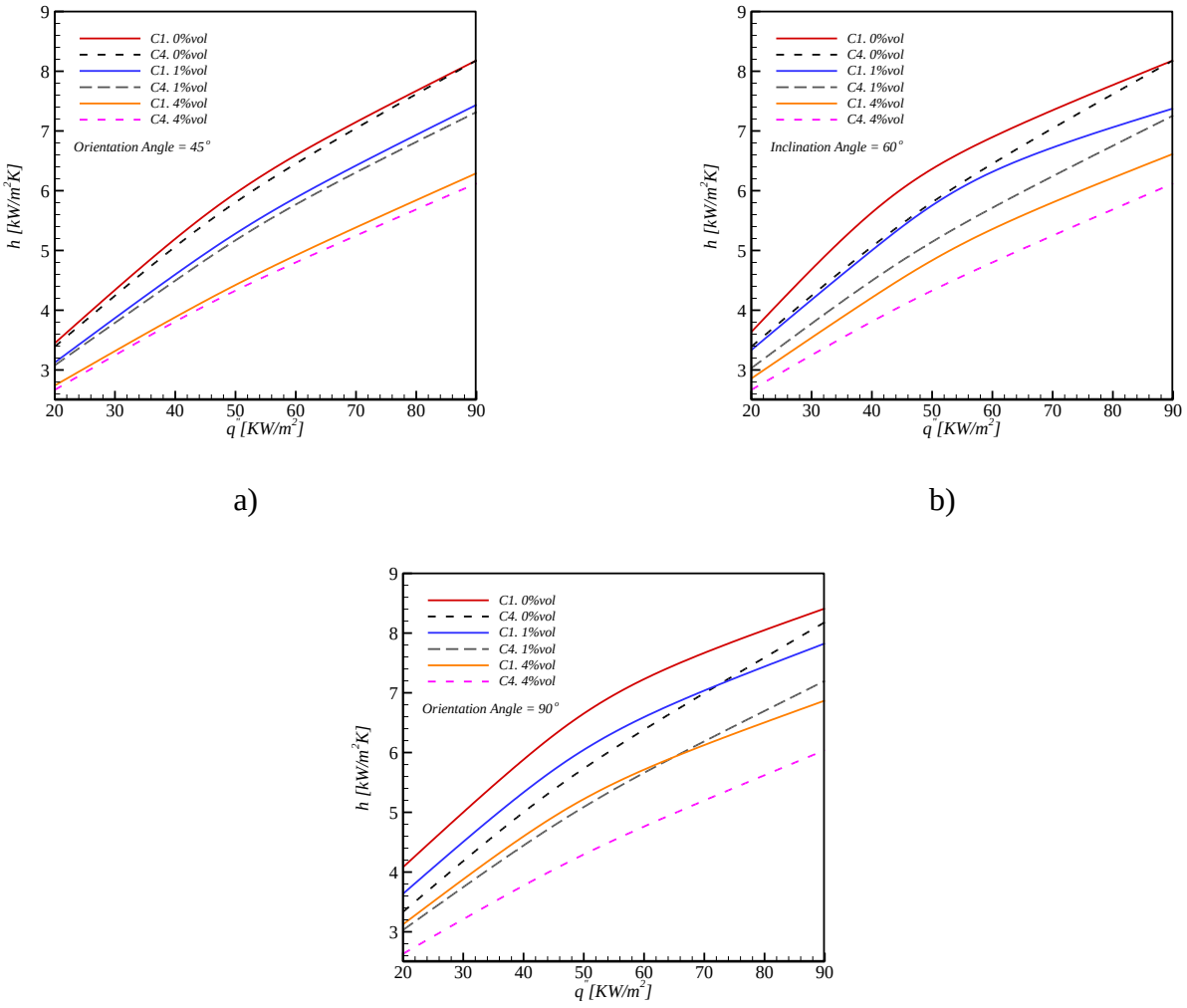

a) b)

c)

Figure 6. Heat transfer coefficient on the surfaces of the top tube (C1) and bottom tube (C4) at different orientation angles with water and alumina nanofluid in pool boiling

The effects of horizontal pitch distances on HTC over the tubes are presented in Figure 11 for different nanoparticles volume fraction. HTC is the highest on the top tube and remains amlost the same on other tubes. When the pitch distance goes beyond the size of the tube diameter, which is 20 mm, HTC reaches its asymptotic value for all the tubes at any nanoparticles volume fraction. As the pitch distance expands, the tubes C4, C3 and C2 behave like an independent and single cylinder and CHT for all of them eventually reaches the same value. This can be attributed to the small sizes of bubbles (less than 1.5 mm), which cannot fill the pitch distance to effect to the laterally spaced tube. It is also observed that the

optimum pitch distance should be chosen between 5 mm to 10 mm, which are 0.25 and 0.5 of the tube diameter. At this distance, HTC reaches its maximum value on all tubes.

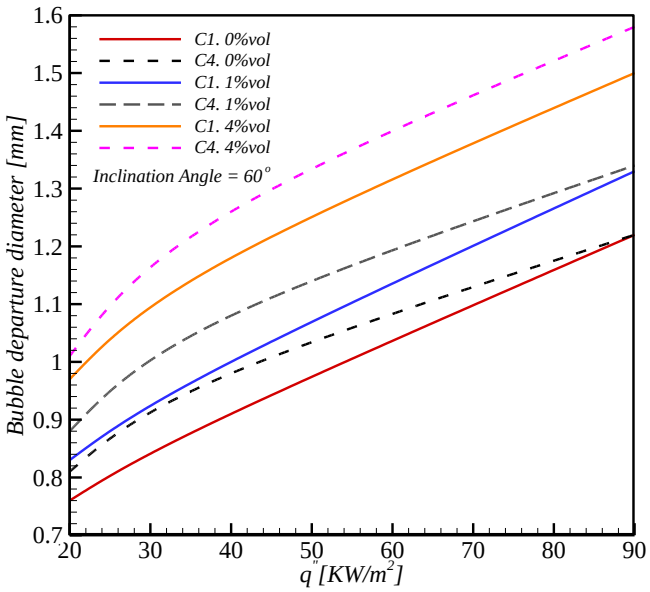

a)

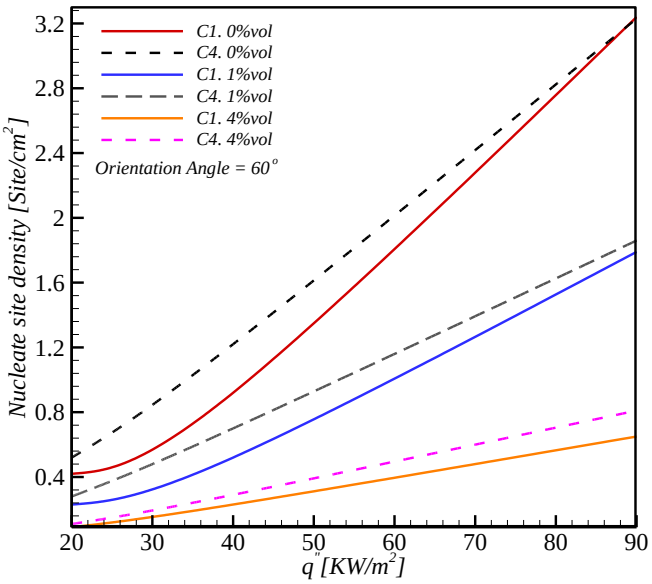

b)

Figure 7. Bubble departure diameter and nucleate site density on the top tube (C1) and bottom tube (C4) for nanofluid pool boiling with different volume fraction

7 Conclusion

Heat transfer features and the percentage of deposition of nanoparticles on heated walls were numerically investigated in a pool boiling flow on a single tube and four-tube bundle. Eulerian-Eulerian multiphase approach was employed to model pool boiling, and the Lagrangian frame was used to track particles during boiling on the surface. New correlations were implemented for bubble departure diameter and nucleate site density from literature. The correlations considered the important effects of nanoparticles, system pressure and surface roughness due to deposited particles. At the first step, the results of the simulations were compared with experimental measurements for alumina nanofluid on a heated cylinder. Then, a tube bundle consisting of four tubes was simulated with different orientation angle and horizontal pitch distances. It was found that particles deposition highly depends on volume fraction and heat flux, reaching the maximum value between 30 KW/m^2 to 60 KW/m^2. The impact of particles deposition on decreasing nucleate site density was found higher than the increase in bubble departure diameter. In the case of the tube bundle, heat transfer coefficient reached its maximum value on the top tube and minimum on the bottom one. The effects of orientation angle on HTC and boiling parameters can be ignored up to 50^o, and then, the sharp changes were observed. Variation of horizontal pitch distance showed that it is possible to find a distance with higher heat transfer for all the tubes, somewhere between 0.25 and 0.5 times of the tube diameter. On the distance larger than the size of the tube diameter, no changes on heat transfer on the tubes were found.

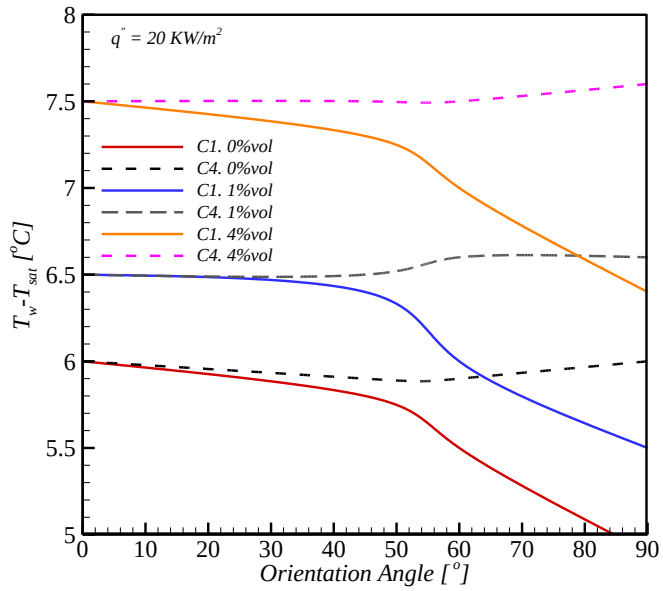

a)

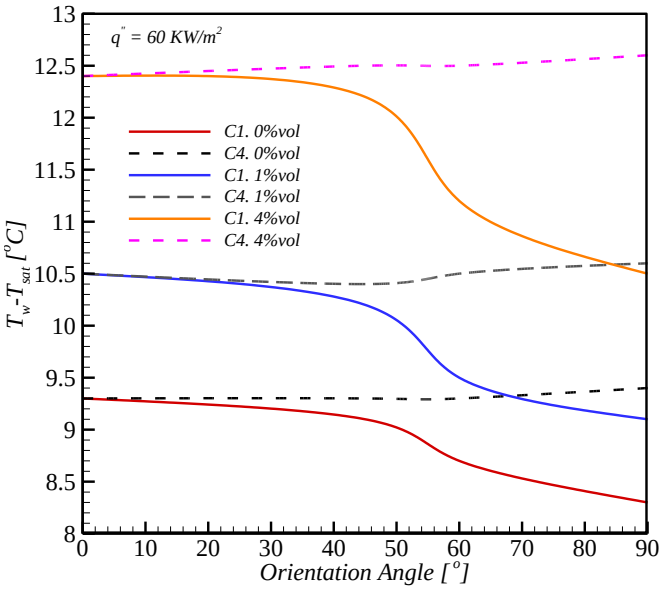

b)

Figure 8. Variation of wall superheat temperature with orientation angle for alumina nanofluid at different volume fraction and heat flux

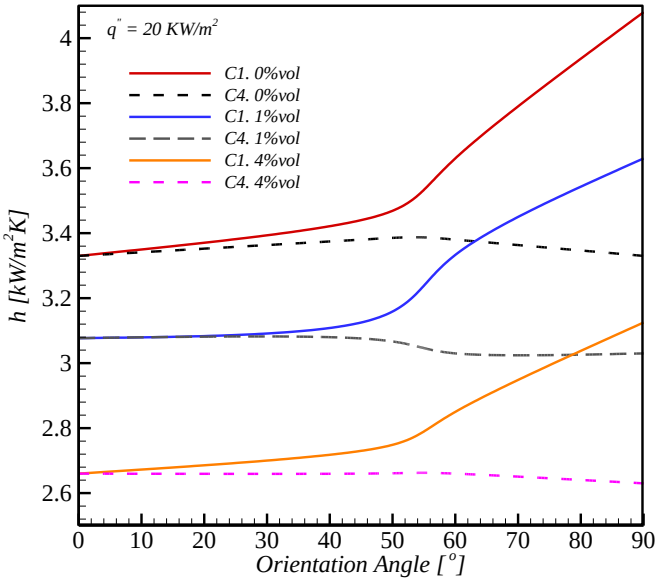

a)

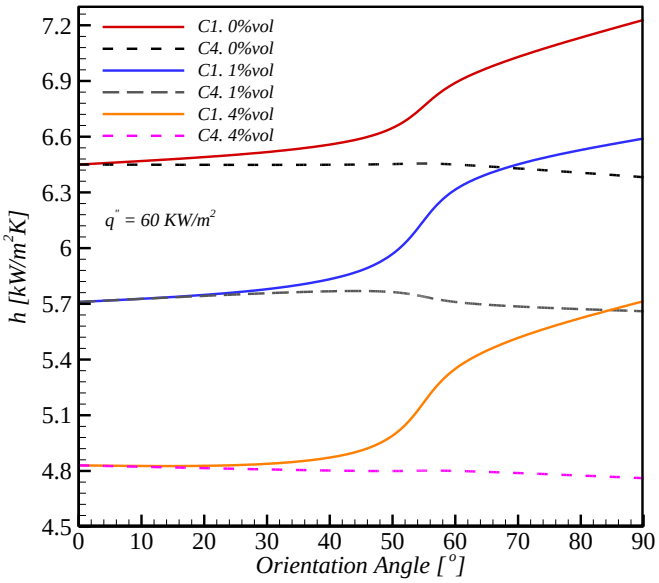

b)

Figure 9. Heat transfer coefficient on the boiling surface versus orientation angle for alumina nanofluid with different volume fraction and heat flux

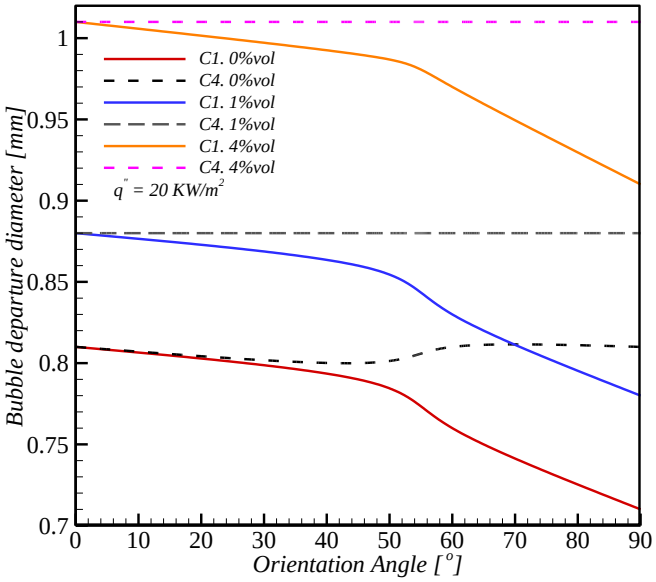

a)

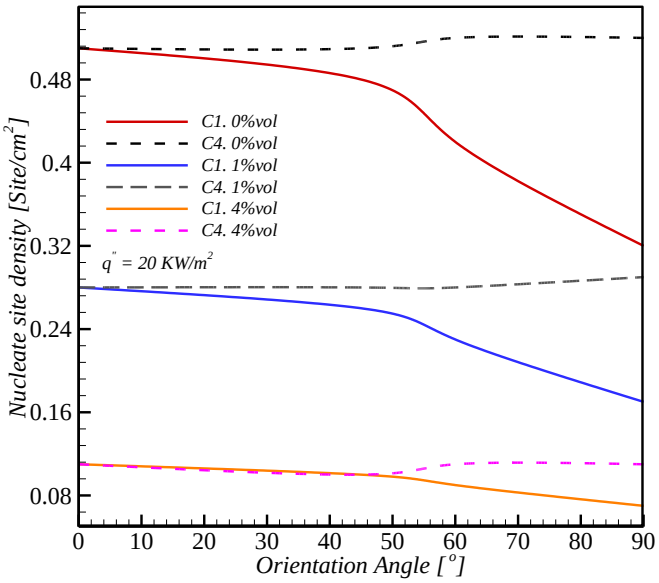

b)

Figure 10. a) Bubble departure diameter and b) nucleate site density versus orientation angle for alumina nanofluid at different volume fraction and heat flux

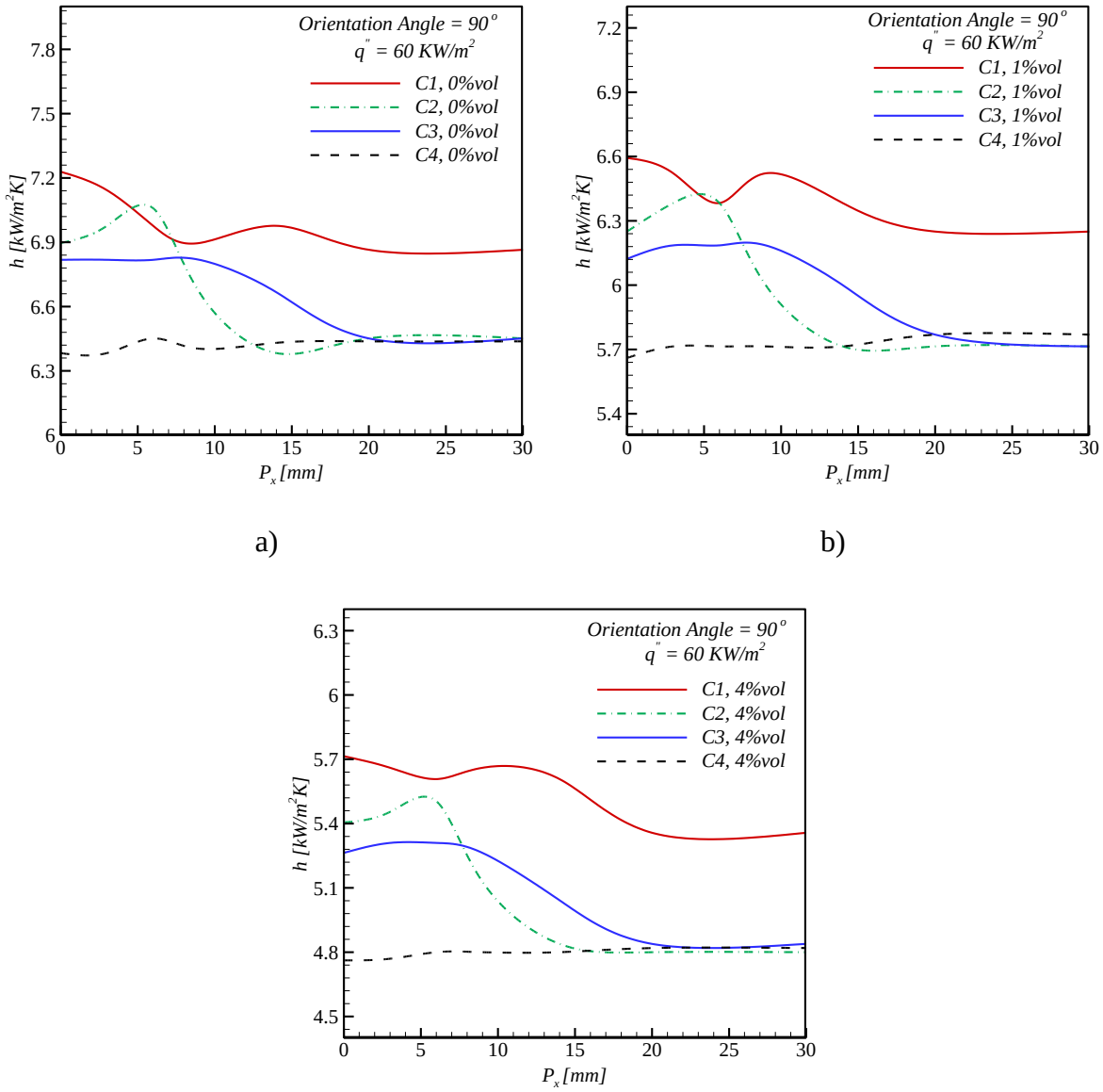

Figure 11. Heat transfer coefficient on the tubes with changes in horizontal pitch distances for alumina nanofluid

Nomenclature

A_i	interfacial area [m^2]
A_p	particle projected area [m^2]
C_L	lift coefficient
C_w	wall lubrication coefficient
C_c	cunningham correction factor
C_D	drag coefficient
C_{ML}	rotational coefficient
C_ω	rotational drag coefficient
C_{qw}	bubble waiting time coefficient
c_p	specific heat (J/kg.K)
d	diameter [m]
d_p	particle diameter [m]
d_w	bubble departure diameter [m]
D_T	thermophoresis diffusion coefficient [m^2/s]
h	heat transfer coefficient [$W/m^2.K$]
h_k	enthalpy [J/kg]
h_{lv}	latent heat of evaporation [J/kg]

I_p	moment of inertia [kg/m^2]
k	Thermal conductivity [W/m.K]
K_B	Boltzmann constant [m^2.kg/^{o}K.s^2]
m_p	particle mass [kg]
M_k	momentum induced by mass exchanged [kg/m^2.s^2]
N_w	nucleate site density
Nu	Nusselt number
n_w	wall normal vector
Pr	Prandtl number
q_k , q_k^t	laminar and turbulent heat flux [W/m^2]
Ra	surface roughness [m]
Re	Reynolds number
Re_p	particle Reynolds number
Re_{ω_p}	angular Reynolds number
Sc_b	Schmidt number
Δt_p	particle time step [s]
V,u	velocity [m/s]

u_i'	fluctuating velocity [m/s]
Greek letters	
α	phase volume fraction
φ	particle volume fraction
Γ_k	Exchanged mass [kg/m^3.s]
$\dot{\gamma}$	shear rate [1/s]
κ	turbulent kinetic energy [m^2/s^2]
μ	viscosity [Pa.s]
μ_t	turbulent viscosity [Pa.s]
ω_p	particle angular velocity [1/s]
Ω	relative particle-liquid angular velocity [1/s]
ρ	density [kg/m^3]
σ	surface tension [N/m]
θ	contact angle
$\Im_k$, $\Im_k^t$	laminar and turbulent shear stress [Pa]
ζ_i	Gaussian white noise random number
ξ	random number
Subscript	

bf	base fluid
k	continues phase
l	liquid
m	mixture
nf	nanofluid
v	vapour
p	particle
sat	saturation
W,s	wall, surface

Reference

[1] D. Yadav, C. Kim, J. Lee, H.H. Cho, Influence of magnetic field on the onset of nanofluid convection induced by purely internal heating, Comput. Fluids. 121 (2015) 26–36. doi:10.1016/j.compfluid.2015.07.024.

[2] Z. Mehrez, M. Bouterra, A. El Cafsi, A. Belghith, Heat transfer and entropy generation analysis of nanofluids flow in an open cavity, Comput. Fluids. 88 (2013) 363–373. doi:10.1016/j.compfluid.2013.09.026.

[3] R. Prasher, P.E. Phelan, P. Bhattacharya, Effect of aggregation kinetics on the thermal conductivity of nanoscale colloidal solutions (nanofluid), Nano Lett. 6 (2006) 1529–

1534. doi:10.1021/nl060992s.

[4] A.T. Utomo, E.B. Haghighi, A.I.T. Zavareh, M. Ghanbarpourgeravi, H. Poth, R. Khodabandeh, B. Palm, A.W. Pacek, The effect of nanoparticles on laminar heat transfer in a horizontal tube, Int. J. Heat Mass Transf. 69 (2014) 77–91. doi:10.1016/j.ijheatmasstransfer.2013.10.003.

[5] K.S. Hwang, S.P. Jang, S.U.S. Choi, Flow and convective heat transfer characteristics of water-based Al2O3 nanofluids in fully developed laminar flow regime, Int. J. Heat Mass Transf. 52 (2009) 193–199. doi:10.1016/j.ijheatmasstransfer.2008.06.032.

[6] D. Liu, L. Yu, Single-phase thermal transport of nanofluids in a minichannel, J. Heat Transfer. 133 (2011) 31009.

[7] M. Mahdavi, M. Sharifpur, H. Ghodsinezhad, J.P. Meyer, A new combination of nanoparticles mass diffusion flux and slip mechanism approaches with electrostatic forces in a natural convective cavity flow, Int. J. Heat Mass Transf. 106 (2017) 980–988. doi:10.1016/j.ijheatmasstransfer.2016.10.065.

[8] W. Duangthongsuk, S. Wongwises, An experimental study on the heat transfer performance and pressure drop of TiO2-water nanofluids flowing under a turbulent flow regime, Int. J. Heat Mass Transf. 53 (2010) 334–344. doi:10.1016/j.ijheatmasstransfer.2009.09.024.

[9] M.A. Khairul, A. Hossain, R. Saidur, M.A. Alim, Prediction of heat transfer performance of CuO/water nanofluids flow in spirally corrugated helically coiled heat exchanger using fuzzy logic technique, Comput. Fluids. 100 (2014) 123–129. doi:10.1016/j.compfluid.2014.05.007.

[10] Y. Hu, H. Li, Y. He, Z. Liu, Y. Zhao, Effect of nanoparticle size and concentration on

boiling performance of SiO2 nanofluid, Int. J. Heat Mass Transf. 107 (2017) 820–828. doi:10.1016/j.ijheatmasstransfer.2016.11.090.

[11] H. Aminfar, M. Mohammadpourfard, M. Sahraro, Numerical simulation of nucleate pool boiling on the horizontal surface for nano-fluid using wall heat flux partitioning method, Comput. Fluids. 66 (2012) 29–38. doi:10.1016/j.compfluid.2012.05.019.

[12] Y. Wang, G.H. Su, Experimental investigation on nanofluid flow boiling heat transfer in a vertical tube under different pressure conditions, Exp. Therm. Fluid Sci. 77 (2016) 116–123. https://vpn.upct.es/science/article/pii/,DanaInfo=www.sciencedirect.com+S0894177716300905.

[13] S.N. Shoghl, M. Bahrami, M. Jamialahmadi, The boiling performance of ZnO, a-Al2O3 and MWCNTs/water nanofluids: An experimental study, Exp. Therm. Fluid Sci. 80 (2017) 27–39.

[14] S.M. You, J.H. Kim, K.H. Kim, Effect of nanoparticles on critical heat flux of water in pool boiling heat transfer, Appl. Phys. Lett. 83 (2003) 3374–3376. doi:10.1063/1.1619206.

[15] S.J. Kim, I.C. Bang, J. Buongiorno, L.W. Hu, Surface wettability change during pool boiling of nanofluids and its effect on critical heat flux, Int. J. Heat Mass Transf. 50 (2007) 4105–4116. doi:10.1016/j.ijheatmasstransfer.2007.02.002.

[16] I.C. Bang, S. Heung Chang, Boiling heat transfer performance and phenomena of Al2O3–water nano-fluids from a plain surface in a pool, Int. J. Heat Mass Transf. 48 (2005) 2407–2419. doi:10.1016/j.ijheatmasstransfer.2004.12.047.

[17] D. Zhu, S. Wu, N. Wang, Thermal Physics and Critical Heat Flux Characteristics of Al

2 O 3 –H 2 O Nanofluids, Heat Transf. Eng. 31 (2010) 1213–1219. doi:10.1080/01457631003733019.

[18] Y. Wang, K.H. Deng, B. Liu, J.M. Wu, G.H. Su, A correlation of nanofluid flow boiling heat transfer based on the experimental results of AlN/H2O and Al2O3/H2O nanoflui, Exp. Therm. Fluid Sci. 5 (2017) 376–383. doi:10.1016/j.ijheatmasstransfer.2014.03.010.

[19] J. Ham, H. Cho, Theoretical analysis of pool boiling characteristics of Al2O3 nanofluid according to volume concentration and nanoparticle size, Appl. Therm. Eng. 108 (2016) 158–171. doi:10.1016/j.applthermaleng.2016.07.058.

[20] Y. Wang, J. Wu, Numerical simulation on single bubble behavior during Al2O3/H2O nanofluids flow boiling using Moving Particle Simi-implicit method, Prog. Nucl. Energy. 85 (2015) 130–139. doi:10.1016/j.pnucene.2015.06.017.

[21] X. Li, S. Chi, P. Cheung, J. Tu, Nucleate boiling of dilute nano fluids- Mechanism exploring and modeling, Int. J. Therm. Sci. 84 (2014) 323–334. doi:10.1016/j.ijthermalsci.2014.05.021.

[22] S.N. Shoghl, M. Bahrami, M.K. Moraveji, Experimental investigation and CFD modeling of the dynamics of bubbles in nanofluid pool boiling, Int. Commun. Heat Mass Transf. 58 (2014) 12–24. doi:10.1016/j.icheatmasstransfer.2014.07.027.

[23] Y. Liu, T. Olewski, L.N. Véchot, Modeling of a cryogenic liquid pool boiling by CFD simulation, J. Loss Prev. Process Ind. 35 (2015) 125–134. doi:10.1016/j.jlp.2015.04.006.

[24] C. Kang, M. Okada, A. Hattori, K. Oyama, Natural convection of water-fine particle suspension in a rectangular vessel heated and cooled from opposing vertical walls (

classication of the natural convection in the case of suspension with a narrow-size distribution), Int. J. Heat Mass Transf. 44 (2001) 2973–2982.

[25] M. Ishii, T. Hibiki, Thermo-fluid dynamics of two-phase flow, Springer Science & Business Media, 2010.

[26] R. Clift, J.R. Grace, M.E. Weber, Bubbles, drops, and particles, Courier Corporation, 2005.

[27] A. Tomiyama, Struggle with computational bubble dynamics, Multiph. Sci. Technol. 10 (1998) 369–405.

[28] S.P. Antal, R.T. Lahey, J.E. Flaherty, Analysis of phase distribution in fully developed laminar bubbly two-phase flow, Int. J. Multiph. Flow. 17 (1991) 635–652.

[29] A.D. Burns, T. Frank, I. Hamill, J.-M. Shi, The Favre averaged drag model for turbulent dispersion in Eulerian multi-phase flows, in: 5th Int. Conf. Multiph. Flow, ICMF, 2004: pp. 1–17.

[30] D.A. Drew, R.T. Lahey, In particulate two-phase flow, 1993.

[31] W.E. Ranz, W.R. Marshall, Evaporation from drops, Chem. Eng. Prog. 48 (1952) 141446.

[32] J. Lavieville, E. Quemerais, S. Mimouni, M. Boucker, N. Mechitoua, NEPTUNE CFD V1. 0 theory manual, NEPTUNE Rep. Nept_2004_L1. 2 (2006).

[33] N. Kurul, M.Z. Podowski, others, On the modeling of multidimensional effects in boiling channels, in: Proc. 27th Natl. Heat Transf. Conf., 1991: pp. 301–314.

[34] V.H. Del Valle, D.B.R. Kenning, Subcooled flow boiling at high heat flux, Int. J. Heat Mass Transf. 28 (1985) 1907–1920.

[35] G. Kocamustafaogullari, M. Ishii, Foundation of the interfacial area transport equation and its closure relations, Int. J. Heat Mass Transf. 38 (1995) 481–493.

[36] G. Kocamustafaogullari, M. Ishii, Interfacial area and nucleation site density in boiling systems, Int. J. Heat Mass Transf. 26 (1983) 1377–1387.

[37] R.J. Benjamin, A.R. Balakrishnan, Nucleation Site Density in Pool Boiling of Saturated Pure Liquids : Effect of Surface Microroughness and Surface and Liquid Physical Properties, Exp. Therm. Fluid Sci. 15 (1997) 32–42.

[38] X. Li, Y. Yuan, J. Tu, A parametric study of the heat fl ux partitioning model for nucleate boiling of nano fl uids, Int. J. Therm. Sci. 98 (2015) 42–50.

[39] V.S. Golorin, B.A. Kol'chugin, E.A. Zakharova, Investigation of the mechanism of nucleate boiling of ethyl alcohol and benzene by means of high-speed motion-picture photography, Heat Transf. Res. 10 (1978) 79–98.

[40] H. Chen, G. Chen, X. Zou, Y. Yao, M. Gong, Experimental investigations on bubble departure diameter and frequency of methane saturated nucleate pool boiling at four different pressures, Int. J. Heat Mass Transf. 112 (2017) 662–675. doi:10.1016/j.ijheatmasstransfer.2017.05.031.

[41] M. Mahdavi, M. Sharifpur, J.P. Meyer, Natural convection study of Brownian nano-size particles inside a water-filled cavity by Lagrangian-Eulerian tracking approach, in: Heat Transf., International Conference on Heat Transfer, Fluid Mechanics and Thermodynamics (HEFAT2016), Costa del Sol, Malaga, Spain, 2016: p. 17.

[42] X. Zheng, Z. Silber-Li, The influence of Saffman lift force on nanoparticle concentration distribution near a wall, Appl. Phys. Lett. 95 (2009) 24–27. doi:10.1063/1.3237159.

[43] B. Oesterle, T.B. Dinh, Experiments on the lift of a spinning sphere in a range of intermediate Reynolds numbers, Exp. Fluids. 25 (1998) 16–22. doi:10.1007/s003480050203.

[44] G.S. McNab, A. Meisen, Thermophoresis in liquids, J. Colloid Interface Sci. 44 (1973) 339–346. doi:10.1016/0021-9797(73)90225-7.

[45] A. Li, G. Ahmadi, Dispersion and Deposition of Spherical Particles from Point Sources in a Turbulent Channel Flow, Aerosol Sci. Technol. 16 (1992) 209–226. doi:10.1080/02786829208959550.

[46] C.J. Van Oss, M.K. Chaudhury, R.J. Good, Interfacial Lifshitz-van der Waals and polar interactions in macroscopic systems, Chem. Rev. 88 (1988) 927–941. doi:10.1021/cr00088a006.

[47] M. Bayazit, Random Walk Model For Motion Of A Solid Particle In Turbulent Open-Channel Flow, J. Hydraul. Res. 10 (1972) 1–14. doi:10.1080/00221687209500016.

[48] J.-S. Shuen, L.-D. Chen, G.M. Faeth, Evaluation of a stochastic model of particle dispersion in a turbulent round jet, AIChE J. 29 (1983) 167–170.

[49] M. Sharifpur, S. Yousefi, J.P. Meyer, A new model for density of nanofluids including nanolayer, Int. Commun. Heat Mass Transf. 78 (2016) 168–174. doi:10.1016/j.icheatmasstransfer.2016.09.010.

[50] M. Corcione, Empirical correlating equations for predicting the effective thermal conductivity and dynamic viscosity of nanofluids, Energy Convers. Manag. 52 (2011) 789–793. doi:10.1016/j.enconman.2010.06.072.

[51] K. Khanafer, K. Vafai, A critical synthesis of thermophysical characteristics of nanofluids, Int. J. Heat Mass Transf. 54 (2011) 4410–4428.

[52] H.P. Meissner, A.S. Michaels, Surface tensions of pure liquids and liquid mixtures, Ind. Eng. Chem. 41 (1949) 2782–2787.

[53] S.K. Das, N. Putra, W. Roetzel, Pool boiling characteristics of nano-fluids, Int. J. Heat Mass Transf. 46 (2003) 851–862.